Excited State Structures and Decay Dynamics of 1,3-Dimethyluracils in Solutions: Resonance Raman and Quantum Mechanical Calculation Study

ARTICLE *in* THE JOURNAL OF PHYSICAL CHEMISTRY B · AUGUST 2013

Impact Factor: 3.3 · DOI: 10.1021/jp403798d · Source: PubMed

7 AUTHORS, INCLUDING:

Xuming Zheng
Zhejiang Sci-Tech University
109 PUBLICATIONS **1,260** CITATIONS
SEE PROFILE

Wei-Hai Fang
Beijing Normal University
233 PUBLICATIONS **4,481** CITATIONS
SEE PROFILE

THE JOURNAL OF PHYSICAL CHEMISTRY B

Article

pubs.acs.org/JPCB

Excited State Structures and Decay Dynamics of 1,3-Dimethyluracils in Solutions: Resonance Raman and Quantum Mechanical Calculation Study

Ming-Juan Li, Ming-Xia Liu, Yan-Ying Zhao, Ke-Mei Pei, Hui-Gang Wang, and Xuming Zheng*

Department of Chemistry and Key Laboratory of Advanced Textiles Material and Manufacture Technology, MOE, Zhejiang Sci-Tech University, Hangzhou, Zhejiang Province, 310023, People's Republic of China

Wei Hai Fang*

Department of Chemistry, Beijing Normal University, Beijing 100875, People's Republic of China

Supporting Information

ABSTRACT: The resonance Raman spectroscopic study of the excited state structural dynamics of 1,3-dimethyluracil (DMU), 5-bromo-1,3-dimethyluracil (5BrDMU), uracil, and thymine in water and acetonitrile were reported. Density functional theory calculations were carried out to help elucidate the ultraviolet electronic transitions associated with the A-, and B-band absorptions and the vibrational assignments of the resonance Raman spectra. The effect of the methylation at N1, N3 and C5 sites of pyrimidine ring on the structural dynamics of uracils in different solvents were explored on the basis of the resonance Raman intensity patterns. The relative resonance Raman intensities of DMU and 5BrDMU are computed at the B3LYP-TD level. Huge discrepancies between the experimental resonance Raman intensities and the B3LYP-TD predicted ones were observed. The underlying mechanism was briefly discussed. The decay channel through the $S_1(^1n\pi^*)/S_2(^1\pi\pi^*)$ conical intersection and the $S_1(^1n\pi^*)/T_1(^3\pi\pi^*)$ intersystem crossing were revealed by using the CASSCF(8,7)/6-31G(d) level of theory calculations.

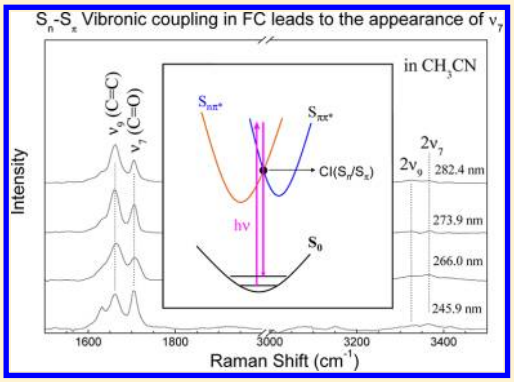

1. INTRODUCTION

Ultraviolet photoexcitation of nucleobases results in photophysical and photochemical processes in their electronic excited states that lead predominantly to photostability with a return to the ground electronic state.[1] Femtosecond spectroscopy experiments have shown that the initial singlet excited state $^1\pi\pi^*$ (S_π) population of pyrimidine nucleobases decays nonradiatively via two distinct internal conversion (IC) pathways.[2−11] One pathway takes place from S_π to the ground state (S_0) via IC on the subpicosecond time scale.[6,7] The other occurs from S_π to a lowest-energy $^1n\pi^*$ (S_n) state with conversion time constants on subpicosecond to picoseconds time scale[8−10] that will either decay to the S_0 state or further produce a minor yield of a triplet excited state (T_1).[11] Accessibility of the internal conversion or conical intersection from S_π to S_n [$CI(S_\pi/S_n)$] has received much experimental and theoretical attention because of its importance in determining the ultrafast excited state dynamics and decay pathways.[12−30] Quantum chemical calculations consistently suggest that the conical intersection between S_π and S_n states are present in coupling regions. S_π/S_n conical intersection is suggested as a mechanism for the rapid nonradiative $S_\pi \rightarrow S_n$ internal conversion observed for nucleobases.[1,16−26]

Resonance Raman spectroscopy has proved to be a powerful tool in studying the structural dynamics in the Franck−Condon (FC) region. The resonance Raman experiments in conjunction with time-dependent wave packet theory in simple model[31,32] have quantitatively been used to examine the initial photochemical reaction coordinates of thymine, uracil, 5-halouracil (5-XU, X = F, Cl, and Br) and 1-methyluracil nucleobases in water.[31−35] The results indicate that the initial excited-state structural dynamics of uracil occurs mostly along the vibrational modes of the in-plane hydrogen-bond angle deformations, the ring stretches, and the carbonyl stretch, while that of thymine occur mostly along a C5═C6 bond lengthening coordinate. Kramers−Kronig transform theory has been employed to calculate the excitation profiles of resonance Raman active vibrations using the absorption band profile of the resonant electronic state. Using the excitation profiles of the five resonant Raman active modes of uracil and the broad electronic absorption band centered at 260 nm as data, Blazej and Peticolas estimated the shifts (Δ_{ej}) in the excited state potential

Received: December 1, 2012
Revised: August 21, 2013
Published: August 23, 2013

energy minimum along the five corresponding normal coordinates Q_j.[36,37] The intensities of the resonance Raman spectra for the S_π excited state of uracil was calculated, ab initio, from the Kramers−Kronig transform theory of resonance Raman scattering.[38]

The time-dependent wave packet theory in simple model and the Kramers−Kronig transform theory of resonance Raman scattering are known to hold only when the following assumptions are met: (1) a single nondegenerate electronic excited state, (2) the Born−Oppenheimer and Condon approximations, (3) no noticeable Duschinsky rotation, and (4) no change in frequency in going from the ground to the excited state. However, when a conical intersection exists in the Franck—Condon region, at least the first two assumptions will break down, and the use of the Kramers−Kronig transform theory or the time-dependent wave packet theory in a simple model will no longer be safe. Therefore clarification of a conical intersection or a curve-crossing or a state mixing between S_π and S_n states in FC region becomes necessary before application of two theories to quantitatively obtain the short-time structural dynamics of nucleobases.

In this paper, we report the resonance Raman spectroscopic and quantum mechanical calculation study on the structural dynamics of 1,3-dimethyluracil (DMU) and 5-bromo-1,3-dimethyluracil (5BrDMU) in water and acetonitrile solvents. CASSCF and TD-B3LYP calculations are used to predict the structures of the lower-lying electronic excited states. The conical intersection point CI(S_π/S_n) and intersystem crossing point ISC(S_n/T_π) are determined for DMU using the CASSCF method. The relative resonance Raman intensities are predicted by using TD-B3LYP calculations for the S_n and S_π states. The results indicate that when CI(S_π/S_n) exists in FC region, the TD-B3LYP predicted resonance Raman intensities deviate severely from the experimental ones, especially in the intensities of the activated vibrational modes due to the $S_\pi-S_n$ vibronic coupling. The excited state decay mechanism of DMU is proposed.

2. EXPERIMENTAL AND COMPUTATIONAL METHODS

DMU (98%), 5BrDMU (98%), uracil (99%), and thymine(97+%) were purchased from Sigma Aldrich and used without further purification. Concentrations of approximately 0.001−0.003 M pyrimidine nucleobases were prepared using spectroscopic or high-performance liquid chromatography (HPLC)-grade solvents of acetonitrile (99.5%, Tedia, USA), and deionized water. The resonance Raman experimental method and apparatus have been described previously[39] so only a short description will be provided here. The harmonics of a nanosecond Nd:YAG laser and their hydrogen Raman shifted laser lines were employed to generate the 299.1, 282.4, 273.9, 266.0, 245.9, and 239.5 nm excitation wavelengths utilized in the resonance Raman experiments. The excitation laser beam used a ∼100 μJ pulse energy loosely focused to a 0.5−1.0 mm diameter spot size onto a flowing liquid stream of sample. A backscattering geometry was employed for collection of the Raman scattered light by reflective optics that imaged the light through a polarizer and entrance slit of a 0.5 m spectrograph and the grating of the spectrograph dispersed the light onto a liquid-nitrogen-cooled charge-coupled device (CCD) mounted on the exit of the spectrograph. The Raman shifts of the resonance Raman spectra were calibrated with the known vibrational frequencies of solvent Raman bands (such as cyclohexane, acetonitrile, etc.). To fully subtract the solvent Raman bands from the resonance Raman spectra of the sample solutions, the pure solvent Raman spectrum at certain excitation wavelength is scaled by a proper factor so that the intensities of the scaled solvent Raman bands matches those of the corresponding bands in the sample resonance Raman spectrum at the same excitation wavelength. Sections of the resonance Raman spectra were fit to a baseline plus a sum of Lorentzian bands to determine the integrated areas of the Raman bands of interest.

The geometry structure optimization and vibrational frequency computation were done using the B3LYP/6-31+G(d) level of theory. The $S_0\rightarrow S_n$ vertical transition energies were estimated at B3LYP-TD/6-31+G(d) levels of theory employing a self-consistent reaction field (SCRF), polarized continuum overlapping spheres model (PCM) and self-consistent isodensity polarizable continuum model (SCIPCM). All of the DFT calculations were done using the Gaussian 09 program.[40]

The excited state gradient at the ground state geometry was calculated using CIS/6-31+G(d) and B3LYP-TD/6-31+G(d) levels. The relative normal mode displacement Δ_i using the short-time approximation is given by $\Delta_i = k\omega_i^{-3/2}(\partial V/\partial Q_i)_0$, where $(\partial V/\partial Q_i)_0$ is the derivative of the excited electronic state potential energy surface with respect to the ith normal mode at the ground state geometry, and can be computed from projection of the potential energy surface of the excited electronic state at the ground state geometry onto the ith ground state vibrational normal mode.[41,42]

The complete active space self-consistent field (CASSCF) theory was used to study the excited state decay mechanism of DMU. The conical intersection and intersystem crossing points between two electronic excited states were computed at CASSCF(8,7)/6-31G* level of theory. Seven active orbitals were used for the CASSCF calculations. An active space with eight electrons in seven orbitals is referred to as CASSCF(8,7) hereafter. For $S_1(^1n\pi^*)/S_2(^1\pi\pi^*)$ conical intersection, seven active orbitals included one n_O, one σ_{C-N}, two π, two π^* and one σ^*_{C-N} orbitals, while for $S_1(^1n\pi^*)/T_1(^3\pi\pi^*)$ intersystem crossing, they included one n_O, three π, two π^* and one Rydberg orbitals.

3. RESULTS AND DISCUSSION

3.1. Electronic Transition of DMU and 5BrDMU in the UV Region. Figure 1 shows the UV absorption spectra of

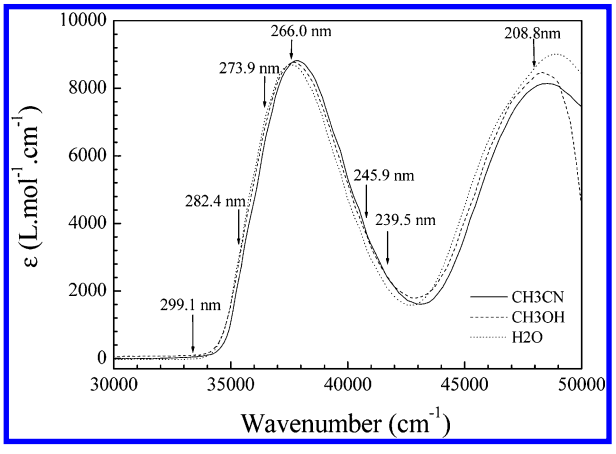

Figure 1. UV absorption spectra of DMU in acetonitrile, methanol, and water.

dx.doi.org/10.1021/jp403798d | J. Phys. Chem. B 2013, 117, 11660−11669

Table 1. B3LYP-TD/6-31+G(d) Computed Electronic Transition Energies in CH_3CN, the Corresponding Orbitals, and the Oscilalator Strengths for DMU and 5BrDMU

state (C_S)	orbitals	character	ΔE/nm calc.[a]	ΔE/nm expt.[b]	oscillator strength f calc.[a]	oscillator strength f expt.[b]
DMU (Singlets)						
S_1 (A″)	36→38(0.684)/36→39(0.116)/34→38(0.106)	$n_{H-1}\rightarrow\pi_L^*/n_{H-1}\rightarrow\pi_{L+1}^*/n_{H-3}\rightarrow\pi_L^*$	250		0.0000	
S_2 (A′)	**37→38(0.678)**/35→39(−0.147)	$\boldsymbol{\pi_H\rightarrow\pi_L^*/\pi_{H-2}\rightarrow\pi_{L+1}^*}$	**250**	**264**	**0.2016**	**0.2369**
S_3 (A′)	35→38(0.687)/37→39(−0.125)	$\pi_{H-2}\rightarrow\pi_L^*/\pi_H\rightarrow\pi_{L+1}^*$	213		0.0709	
S_4 (A″)	34→38(0.564)/36→39(0.355) 34→39(−0.180)/36→38(−0.138)	$n_{H-3}\rightarrow\pi_L^*/n_{H-1}\rightarrow\pi_{L+1}^*$ $n_{H-3}\rightarrow\pi_{L+1}^*/n_{H-1}\rightarrow\pi_L^*$	210		0.0000	
S_5 (A′)	**37→39(0.678)**/35→38(0.119)	$\boldsymbol{\pi_H\rightarrow\pi_{L+1}^*/\pi_{H-2}\rightarrow\pi_L^*}$	**205**	**206**	**0.1587**	**0.3695**
DMU (Triplets)						
T_1 (A′)	33→38(−0.12)/37→38(0.69)	$/\pi_H\rightarrow\pi_L^*$	370		0.0000	
T_2 (A″)	34→38(−0.14)/36→38(0.67)/36→40(0.15)	$n_{H-3}\rightarrow\pi_L^*/n_{H-1}\rightarrow\pi_L^*/n_{H-1}\rightarrow\pi_{L+2}^*$	289		0.0000	
T_3 (A′)	35→38(0.60)/37→40(−0.31)	$\pi_{H-2}\rightarrow\pi_L^*/\pi_H\rightarrow\pi_{L+2}^*$	276		0.0000	
T_4 (A′)	**37→40(0.59)/35→38(0.31)/35→40(0.21)**	$\boldsymbol{\pi_H\rightarrow\pi_{L+2}^*/\pi_{H-2}\rightarrow\pi_L^*/\pi_{H-2}\rightarrow\pi_{L+2}^*}$	**241**		**0.0000**	
T_5 (A″)	34→38(0.40)/34→40(−0.28) 36→38(0.17)/36→40(−0.38)	$n_{H-3}\rightarrow\pi_L^*/n_{H-3}\rightarrow\pi_{L+2}^*$ $n_{H-1}\rightarrow\pi_{L+2}^*/n_{H-1}\rightarrow\pi_L^*$	225		0.0000	
5BrDMU						
S_1 (A′)	**54→55(0.691)**/52→57(−0.114)	$\boldsymbol{\pi_H\rightarrow\pi_L^*/\pi_{H-2}\rightarrow\pi_{L+2}^*}$	**272**	**280**	**0.1992**	**0.2335**
S_2 (A″)	53→55(0.633)/54→56(−0.259) 50→55(0.117)/53→57(0.100)	$n_{H-1}\rightarrow\pi_L^*/\pi_H\rightarrow\sigma_{C-Br}^*$ $n_{H-4}\rightarrow\pi_L^*/n_{H-1}\rightarrow\pi_{L+2}^*$	251		0.0002	
S_3 (A″)	54→56(0.650)/53→55(0.250)	$\pi_H\rightarrow\sigma_{C-Br}^*/n_{H-1}\rightarrow\pi_L^*$	247		0.0005	
S_4 (A′)	52→55(0.668)/54→57(−0.199)	$\pi_{H-2}\rightarrow\pi_L^*/\pi_H\rightarrow\pi_{L+2}^*$	217		0.1098	
S_5 (A″)	51→55(0.691)/53→57(−0.102)	$n_{H-3}\rightarrow\pi_L^*/n_{H-1}\rightarrow\pi_{L+2}^*$	216		0.0001	
S_6 (A′)	**54→57(0.668)**/52→55(0.201)	$\boldsymbol{\pi_H\rightarrow\pi_{L+2}^*/\pi_{H-2}\rightarrow\pi_L^*}$	**214**	**210**	**0.1573**	**0.2599**

[a]B3LYP-TD/6-31+G(d) computed in acetonitrile. [b]Taken from the spectrum in acetonitrile.

DMU in acetonitrile, methanol and water with the excitation wavelengths for the resonance Raman experiments indicated above the curves. The spectra display two absorption bands, which are broad and featureless. Table 1 lists the B3LYP-TD/6-31+G(d) computed electronic transition energies, the corresponding orbitals, and the oscillator strengths. The calculated results show two transition-allowed absorption bands at 247 nm (f = 0.1495) and 201 nm (f = 0.1273) respectively, which correlate with the experimental bands at 264 nm (f = 0.2369) (A-band) and 206 nm (f = 0.3695) (B-band). The band shape and the λ_{max} for the experimental UV absorption spectrum in acetonitrile are similar to those in water or methanol. This suggests the major electronic transitions associated with the A-, and B-band absorptions are not much affected by the solvents.

Figure 2 displays the molecular orbitals associated with the singlet electronic transitions of DMU in UV spectral region. Orbitals 37, 36 and 38, 40 are respectively π and π^* molecular orbitals, and are designed as π_H (HOMO, the highest occupied molecular orbital), π_{H-2} and π_L^* (LUMO, the lowest unoccupied molecular orbital), π_{L+1}^*. Orbitals 36 and 34 are two nonbonding orbitals n_{H-1} and n_{H-3}, while orbital 39 is a diffuse orbital with major amplitude across three hydrogen atoms of methyl group and two hydrogen atoms associated with C5═C6 double bond. Therefore the A-, and B-band absorptions are respectively assigned as $\pi_H\rightarrow\pi_L^*/\pi_{H-2}\rightarrow\pi_{L+2}^*/\pi_{H-2}\rightarrow\pi_L^*$ and $\pi_H\rightarrow\pi_{L+2}^*$ transitions. The A-band absorption of DMU display λ_{max} = 266 nm in water and is red-shifted 7 nm relative to λ_{max} = 259 nm for uracil due to the hyper conjugation of methyl group with π_H (see orbital 37 of DMU in Figure 2).

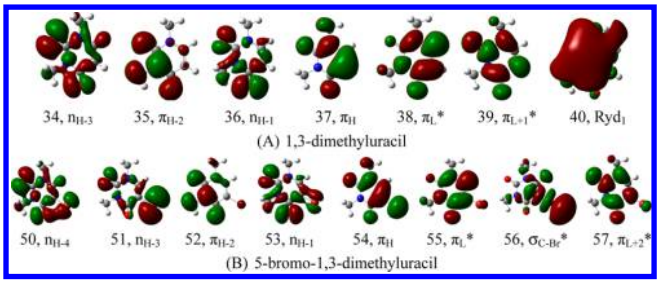

Figure 2. Molecular orbitals of DMU (A) and 5BrDMU (B) associated with the electronic transitions in Table 1

The UV absorption spectra of 5BrDMU in acetonitrile, methanol, and water are in profile very similar to those of DMU except for the red-shifts of λ_{max} for A-, and B-band absorptions. For example, λ_{max} = 280 nm for 5BrDMU in acetonitrile is red-shifted about 16 nm relative to the corresponding λ_{max} = 264 nm for DMU. The explanation is that the energy of the orbital 54 (Figure 2) for 5BrDMU increases relative to that of the orbital 37 for DMU due to the antibonding interaction between p_z orbital of Br and π orbital of DMU moiety, while the energy of orbital 55 is not much affected by Br substitution according to Figure 2 and Table 1 as well as the calculated energies of molecular orbitals. Similar to DUM, the major electronic transitions associated with the A-, and B-band absorptions are also not very much affected by the solvents.

3.2. Vibrational Assignments . There has been no literature report on the vibrational assignments of DMU and 5BrDMU. Figure 3 shows the FT-Raman and FT-IR as well as the computed Raman spectra of DMU and 5BrDMU with the frequency values indicated above the spectra. Table 2 presents the B3LYP/6-31+G(d) calculated and the experimental FT-Raman and resonance Raman observed vibrational frequencies as well as the potential energy distribution (PED%) and the approximate descriptions of the vibrational modes for DMU and 5BrDMU. Both DMU and 5BrDMU possess 48 normal

dx.doi.org/10.1021/jp403798d | J. Phys. Chem. B 2013, 117, 11660−11669

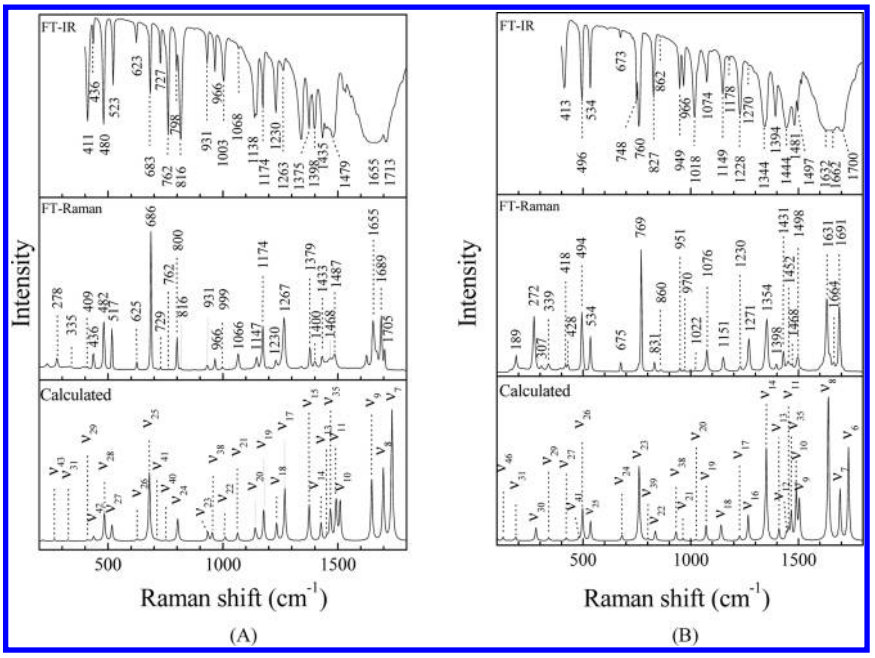

Figure 3. FT-Raman, FT-IR, and B3LYP/6-31+G(d) computed Raman spectra of DMU (A) and 5BrDMU (B) with the frequency values indicated.

modes with 31 and 17 modes being respectively in A′ and A″ irreducible representations, and all in Raman and IR active. Among 25 calculated A′ vibrational modes in 0−1800 cm^{-1} spectrum region, 21 vibrational modes are observed in the solid state Raman spectrum. Figure 3 and Table 2 and Table S1 show that the experimental vibrational bands in 0−1400 cm^{-1} frequency region can be fitted reasonably well by the calculated ones for DMU and 5BrDMU. The experimental vibrational bands in 1500−1800 cm^{-1} region for DMU and 5BrDMU are respectively assigned based on the FT-Raman, FT-IR and the resonance Raman. The experimental FT-Raman spectrum of DMU in solid state displays two moderate intense bands at 1689 and 1655 cm^{-1} and one weak band at 1705 cm^{-1}, while the experimental 266.0 nm resonance Raman spectrum in acetonitrile shows one strong band at 1664 cm^{-1} and one weak band at 1708 cm^{-1}. The experimental FT-IR spectrum of DMU presents a broad intense band at 1655 cm^{-1} and a sharp shoulder band at 1713 cm^{-1}. Therefore, the bands at 1655 and 1705 cm^{-1} in the FT-Raman (or 1655 and 1713 cm^{-1} in FT-IR spectrum) and the bands at 1664 and 1708 cm^{-1} in the 266.0 nm resonance Raman spectrum are respectively assigned to the calculated modes ν_9 (1637 cm^{-1}) and ν_7 (1727 cm^{-1}), while the band at 1689 cm^{-1} in FT-Raman spectrum is assigned to ν_8 (1687 cm^{-1}). Similarly the bands at ∼1631, 1664, and 1691 cm^{-1} in the experimental FT-Raman and FT-IR spectra of 5BrDMU or the bands at 1631, 1659, and 1708 cm^{-1} in the 266.0 nm resonance Raman spectra of 5BrDMU in acetonitrile are respectively assigned to the calculated modes ν_8 (1640 cm^{-1}), ν_7 (1694 cm^{-1}), and ν_6 (1733 cm^{-1}).

3.3. Resonance Raman Spectra and Structural Dynamics of DMU and 5BrDMU. We have measured the A-band resonance Raman spectra of DMU and 5BrDMU at five excitations (299.1, 282.4, 273.9, 266.0, 245.9, 239.5 nm) that cross the whole absorption band and one excitation at 208.8 nm that is at the maximum of the B-band absorption. The intensity patterns for the A-band resonance Raman spectra at five excitations are similar to one another. Figure 4 shows only the overview of the 266.0 nm (and 282.4 nm) resonance Raman spectrum of DMU (and 5BrDMU) in acetonitrile, methanol, and water with tentative vibrational assignments indicated for larger Raman features. Figure S1 displays the overview of the 299.1, 282.4, 273.9, 266.0, 245.9, 239.5, and 208.8 nm Resonance Raman spectra of DMU in acetonitrile and water. The intensity pattern for each A-band resonance Raman spectrum in acetonitrile is similar to one another, but very different than that of the B-band one. Since the intensity of ν_{15}, which is the most intense Raman band in the 208.8 nm (B-band) resonance Raman spectra, occupy only a minor intensity in the A-band resonance Raman spectra, we expect that the preresonance contribution of B-band absorption to the A-band resonance Raman intensities of ν_7, ν_8, ν_9, $\nu_{17} \sim \nu_{26}$ is negligible. Thus the intensity pattern of the 282.4 and 266.0 nm resonance Raman spectra as shown in Figures 4 and S1 reflect mostly the A-band structural dynamics. The Raman band labels in the Figure 4 only give the largest Raman band contributions to each Raman feature due to limited resolution of the solution phase spectra. Most of the A-band resonance Raman features can be assigned as 14 FC active modes: ν_7, ν_8, ν_9, ν_{13}, ν_{15}, ν_{17}, ν_{18}, ν_{19}, ν_{21}, ν_{22}, ν_{23}, ν_{24}, ν_{25}, ν_{26}. Similarly, most of the A-band resonance Raman features of 5BrDMU can be assigned as 13 FC active modes: ν_6, ν_7, ν_8, ν_{11}, ν_{13}, ν_{14}, ν_{16}, ν_{18}, ν_{19}, ν_{20}, ν_{25}, ν_{26}, ν_{27}. Solvents do not affect significantly the A-band short-time structural dynamics of DMU or 5BrDMU since the intensity patterns are in general very similar to each other, as shown in Figure 4.

The A-band resonance Raman spectra of DMU in three solvents indicate that the excited state structural dynamics has significant multidimensional character with the largest contribution in the C5═C6 stretch mode ν_9 and the CH_3 wag mode ν_{17} (mostly for carbon atom 9) since their overtones and combination bands with the remaining modes occupy most of the Raman intensity. The moderate band intensities in the A-band resonance Raman spectra come from the C2═O/C4═O symmetric stretch mode ν_7, the C2═O/C4═O antisymmetric stretch+ C5═C6 stretch mode ν_8, the (N3/N1)-CH_3 umbrella mode ν_{13}, the C5H/C6H in-plane bend mode ν_{19}, the (N3/

dx.doi.org/10.1021/jp403798d | J. Phys. Chem. B 2013, 117, 11660−11669

Table 2. Experimentally Observed and B3LYP/6-31+G(d) Computed Vibrational Frequencies of DMU

	calc (cm^{-1})		expt (cm^{-1})				
	[a]	[b]	FT-Raman	FT-IR	R.R.[c]	descriptions	assignment, PED (%)
A′ υ_1	3260	3115	3095m	3095s		C5H/C6H stretch	νC5H (65)+ νC6H (13)
υ_2	3220	3078	3047w	3045vw		C6H/C5H stretch	νC6H (59)+ νC5H (11)
υ_3	3203	3062				(N3)-CH_3 asym stretch	ν(N3)-CH (48)+ ν(N3)-CH_2 (29)
υ_4	3168	3029	3028w	3026vw		(N1)-CH_3 asym stretch	ν(N1)-CH (41)+ ν(N1)-CH_2 (35)
υ_5	3082	2948				(N3)-CH_3 sym stretch	ν(N3)-CH_3 (86)
υ_6	3077	2943	2958s	2960m		(N1)-CH_3 sym stretch	ν(N1)-CH_3 (87)
υ_7	1772	1713	1705w	1713w	1708w	C2═O/C4═O sym stretch	νC4═O (42)+ νC2═O (40)
υ_8	1733	1667	1689s			C2═O/C4═O asym stretch+ C5═C6 stretch	νC2═O (33)+ νC4═O (30)+ νC5═C6 (26)
υ_9	1681	1627	1655s	1651w	1664vs	C5═C6 stretch+ C6−H in-plane bend	νC5═C6 (42)+ δC6H (15)
υ_{10}	1539	1493				(N1)-CH_3 scissor	(N1)-CH_2 scissor (60) + δ(N1)-CH (10)
υ_{11}	1522	1477	1487w	1479m		(N3)-CH_3 scissor	(N3)-CH_2 scissor (64)
υ_{12}	1491	1448				(N1)-CH_3 umbrella+ C5H in-plane bend	(N1)-CH_3 umbrella (48)+ δC5H (10)
υ_{13}	1479	1437	1433w	1435m	1444s	(N1/N3)-CH_3 umbrella	(N3)-CH_3 umbrella (34) + (N1)-CH_3 umbrella (27)
υ_{14}	1453	1412	1400vw	1398m		(N1/N3)-CH_3 umbrella+ C5H in-plane bend	(N3)-CH_3 umbrella (34) + (N1)-CH_3 umbrella (25) + δC5H (10)
υ_{15}	1400	1362	1379m	1375m	1379w	(N3)-CH_3 umbrella + N1C2N3 asym stretch+ C5H/C6H in-plane bend	(N3)-CH_3 umbrella (17) + νN1C2N3 (14) + δC5H (10) + δC6H (10)
υ_{16}	1370	1334				(N1)-CH_3 wag+ C6H in-plane bend	ρ_w (N1)-CH_2 (22) + δC6H (15)
υ_{17}	1291	1260	1267s	1263w	1269s	(N3)-CH_3 wag+ C2N3C4 asym stretch	ρ_w (N3)-CH_2 (37) + δ(N3)-CH (11) + νC2N3C4 (11)
υ_{18}	1254	1225	1230vw	1230s	1237vvw	N1C/N3C sym stretch+ C5H in-plane bend	νN1C (26) + νN3C (16)+ δC5H (12)
υ_{19}	1196	1170	1174s	1174m	1163m	C5H/C6H in-plane bend	δC5H (25) + δC6H (11)
υ_{20}	1157	1133	1147w	1138s	1144vw	(N1)-CH_3 wag + N3C4C5 asym stretch+ C6H bend	ρ_w(N1)-CH_2 (27) + νN3C4C5 (15) + δC6H (10)
υ_{21}	1079	1060	1066m	1068vw	1068m	(N1/N3)-CH_3 wag+ N1C2N3 asym stretch	ρ_w(N1)-CH_2 (21) + ρ_w (N3)-CH_2 (13) +νN1C2N3 (13)
υ_{22}	1023	1007	999vw	1003s	1007w	(N1/N3)-CH_3 wag	ρ_r (N3)-CH_2 (21) + ρ_r (N1)-CH_2 (16)
υ_{23}	946	934	931vw	931m	932w	(N3)-CH_3 wag+ C4N3C sym stretch	ρ_w (N3)-CH_2 (17)+ νC4N3C (13)
υ_{24}	810	806	800m	798w	807m	ring deformation	ring deform (100)
υ_{25}	683	686	686vs	683s	685w	ring breath	ring breath (100)
υ_{26}	628	635	625vw	623m	622w	ring in-plane bend	δ ring (100)
υ_{27}	515	528	517s	523s		ring deformation	ring deform (100)
υ_{28}	481	496	482s	480vs		ring deformation	ring deform (100)
υ_{29}	405	424	409vw	411s		C2═O scissor+ (N3)-CH_3 in-plane bend	C2═O scissor (31)+ δ(N3)-CH_3 (15)
υ_{30}	365	388				(N3/N1)-CH_3 in-plane bend+ C2═O in-plane bend	δ N3-CH_3 (34)+ δ (N1)-CH_3 (31)+ δC2═O (14)
υ_{31}	316	341	335vw			(N1/N3)-CH_3 in-plane bend	δ (N1)-CH_3 (38)+ δ (N3)-CH_3 (25)
A″ υ_{32}	3146	3008				(N1)-CH_3 asym stretch	ν(N1)-CH_2 (67)
υ_{33}	3145	3007	3008w	3005w		(N3)-CH_3 asym stretch	ν(N3)-CH_2 (67)
υ_{34}	1519	1474				(N3)-CH_3 twist	ρ_t (N3)-CH_2 (51)+ γ(N3)-CH (43)
υ_{35}	1496	1453	1468vw	1462vw		(N1)-CH_3 twist	ρ_t (N1)-CH_2 (51)+ γ(N1)-CH (42)
υ_{36}	1164	1140				(N3)-CH_3 rock	ρ_r (N3)-CH_2 (44)+ γ(N3)-CH (19)
υ_{37}	1159	1135				(N1)-CH_3 rock	ρ_r (N1)-CH_2 (44)+ γ(N1)-CH (19)
υ_{38}	965	952	966w	966m		C6H/C5H out-of-plane bend	γC6H (54)+ γC5H (33)
υ_{39}	811	807				C5H/C6H out-of-plane bend+ C4 out-of-plane bend	γC5H (34)+ γC4 (31)+ γC6H (33)
υ_{40}	756	755	762vw	762vs		C2 out-of-plane bend	γC2 (75)
υ_{41}	714	716	729vw	727m		C4 out-of-plane bend + C5H/C6H out-of-plane bend	γC4 (43)+ γC5H (26)+ γC6H (12)
υ_{42}	433	451	436m	436w		C6H out-of-plane bend+ C5/N3 out-of-plane bend	γC6H (29)+ γC5 (25)+ γN3 (18)
υ_{43}	257	283	278w			N1-C2-N3 twist	ρ_t N1C2N3 (63)
υ_{44}	205	236				N1-C2N3 torsion	τ N1C2N3 (73)
υ_{45}	131	166				(N1/N3)-CH_3 out-of-plane bend	γ(N3)-CH_3 (49)+ γ(N1)-CH_3 (17)
υ_{46}	110	146				(N1/N3)-CH_3 out-of-plane bend	γ(N1)-CH_3 (40)+ γ(N3)-CH_3 (21)
υ_{47}	103	140				(N1/N3)-CH_3 rock	ρ_r (N1)-CH_3 (60)+ ρ_r (N3)-CH_3 (32)
υ_{48}	86	124				(N1/N3)-CH_3 rock	ρ_r (N3)-CH_3 (58)+ρ_r (N1)-CH_3 (32)

[a]B3LYP/6-31+G(d) calculated. [b]Scaled = 42.76 + 0.9425 × calculated. [c]Data from 266.0 nm resonance Raman spectrum in acetonitrile solvent; vs: very strong;s: strong; m: middle; w: weak; vw: very weak; sh: shoulder; ν: stretching; sym: symmetry; asym: asymmetry; δ: in-plane bending; γ: out-

dx.doi.org/10.1021/jp403798d | J. Phys. Chem. B 2013, 117, 11660−11669

Table 2. continued

of-plane bending; ρ_w: wagging; ρ_r: rocking; ρ_t: twisting; τ: torsion; Ring deform: ring deformation; PED: potential energy distribution, only contributions larger than 10% were given.

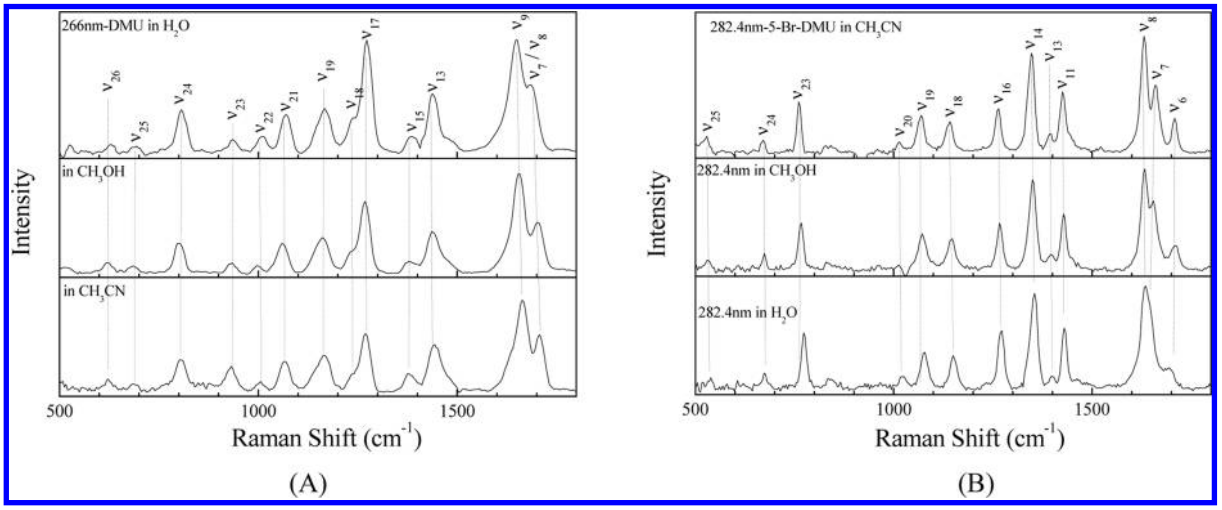

Figure 4. (A) Overall view of the 266.0 nm resonance Raman spectra of DMU in acetonitrile (bottom), methanol (middle) and water (top) with tentative vibrational assignments indicated for larger Raman features. (B) Overall view of the 282.4 nm resonance Raman spectra of 5BrDMU in acetonitrile (bottom), methanol (middle) and water (top) with tentative vibrational assignments indicated for larger Raman features.

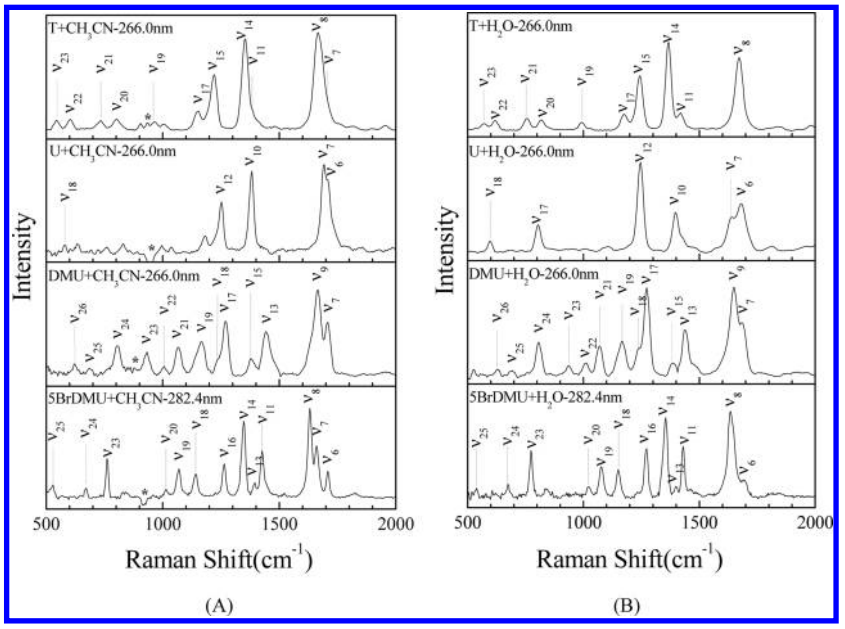

Figure 5. Comparison of the A-band resonance Raman spectra of thymine, uracil, DMU, and 5BrDMU in acetonitrile (A) and water (B).

N1)-CH_3 wag+ N1-C2-N3 asym stretch mode ν_{21}, and the ring deformation mode ν_{24}. Similarly, the A-band resonance Raman spectra of 5BrDMU in three solvents indicates that the excited state structural dynamics is mostly along the reaction coordinates of C5═C6 stretch mode ν_8 and the N1-C2/C2-N3/N1-C6/C6-C5 stretch+ (N3)-CH_3 umbrella + C6H in-plane bend mode ν_{14}. The structural dynamics along the C5═C6 reaction coordinate for DMU and 5BrDMU consists well with the major electronic transitions associated with the corresponding A-band absorption since the $\pi_H \rightarrow \pi_L^*$ transition (see orbitals 37 and 38 for DMU or 54 and 55 for 5BrDMU in Figure 2) weakens C5═C6 bond greatly. The significant structural dynamics along the CH_3 wag mode ν_{17} (mostly for carbon atom 9) for DMU in acetonitrile and water is partially in an agreement with the $\pi_{H-2} \rightarrow \pi_{L+2}^*$ and $\pi_{H-2} \rightarrow \pi_L^*$ electronic transitions since they change somewhat the electronic density in (N3)-CH_3 group (see orbitals 35, 38, and 40 in Figure 2). However, the significant structural dynamics along the C2═O/C4═O symmetric stretch mode ν_7 and the C2═O/C4═O antisymmetric stretch + C5═C6 stretch mode ν_8 for DMU is not in accordance with the expected minor changes in the electronic density around the moiety of C2═O/C4═O as induced by the $\pi_H \rightarrow \pi_L^*/\pi_{H-2} \rightarrow \pi_{L+2}^*/\ \pi_{H-2} \rightarrow \pi_L^*$ electronic transitions.

3.4. Comparison of the A-Band Structural Dynamics of DMU, 5BrDMU, Uracil, and Thymine. To better understand the effect of the substitution and solvent polarity/hydrogen bonding interaction on the excited state reaction

dx.doi.org/10.1021/jp403798d | J. Phys. Chem. B 2013, 117, 11660−11669

dynamics of uracils, we have obtained the additional resonance Raman spectra of thymine and uracil in acetonitrile. The comparison of the A-band resonance Raman spectra of thymine, uracil, DMU, and 5BrDMU in acetonitrile and water is included in Figure 5. The spectra have been intensity corrected and solvent subtracted. The tentative assignments for the larger Raman band features are also shown. The top panel of Figure 5A shows that most of the resonance Raman features of thymine in water solution can be assigned to the fundamentals, overtones, and combination bands of approximately 10 A′ vibrational modes ν_{23}, ν_{22} ν_{21}, ν_{20}, ν_{19}, ν_{17}, ν_{15}, ν_{14}, ν_{11}, and ν_{8}. Similarly, all of the FC modes for the A-band resonance Raman spectra of uracil, DMU, and 5BrDMU in water and acetonitrile are in A′ irreducible representation. This indicates that the initial excited state structural dynamics appears to evolve in a symmetric way with little if any out-of-plane motion and there is no significant vibronic coupling between the A′ and A″ states that is noticeable in the FC region. Solvent polarity and hydrogen bonding interaction do not noticeably change the feature.

The resonance Raman intensity pattern of thymine in acetonitrile as shown in the top panels of Figure 5 is very similar to that of thymine in water. This suggests that the short-time structural dynamics of thymine along the major reaction coordinates in both solvents are about the same. The relative intensities of the major bands of ν_8/ν_7, ν_{14}, and ν_{15} for thymine in acetonitrile look similar to those of ν_7/ν_6, ν_{10} and ν_{12} for uracil, but this does not ensure that the major structural dynamics of thymine is similar to that of uracil in acetonitrile since the normal mode descriptions between ν_{10}/ν_{12} for uracil and ν_{14}/ν_{15} for thymine are noticeably different. Different from thymine, the major structural dynamics along the ν_7/ν_6, ν_{10} and ν_{12} for uracil in acetonitrile is very different than those in water according to the intensity patterns as shown in the second top panels of Figure 5. This indicates that the C5 methylation of uracil differentiates significantly the initial structural dynamics between uracil and thymine in water. It appears that the C5−H group is a key structural factor that manipulates the differentiation of the initial structural dynamics and the subsequent formation of CPDs between uracil and thymine only in water environment.

The methylation of N3 and N1 significantly differentiate the structural dynamics between uracil and DMU in both solvents since the initial structural dynamics of DMU is along 13 vibrational modes, while that of uracil in acetonitrile and water are respectively along 5 and 6 modes. That the considerable Raman intensities are partitioned into the methyl-related modes ν_{13}, ν_{15}, ν_{17}, ν_{21}, ν_{22}, ν_{23} for DMU, as is similar for N1-methylthymine,[43] indicates that the N3 and/or N1 methylation is another efficient way to alter the structural dynamics of uracil. It makes the short-time structural dynamics of the methylated uracils in water and acetonitrile similar. A similar case is also found for 5BrDMU, where the considerable Raman intensities are partitioned into a number of methyl-related modes. The A-band resonance Raman spectra of DMU and 5BrDMU are different in nature since both the relative intensity patterns and the normal mode descriptions for some modes are different. This suggests that the substitution of Br atom to C5 position noticeably changes the short-time structural dynamics of DMU, and this is analogous to the case between uracil and 5-chlorouracil.[35]

3.5. TD-B3LYP Computed Relative Resonance Raman Intensities of DMU and 5BrDMU. The A-band resonance Raman spectra of DMU in water and acetonitrile are clearly dominated by fundamental transitions at all wavelengths, as shown in Figure 4. This is the signature that the Raman process is dominated by the very short time scattering probably due to solvent induced damping. In this case, the relative band intensities in a resonance Raman spectrum depend on the relative magnitude of the displacements of the normal modes in question in the excited electronic state. This means that the only feature that is being revealed about the resonant excited state is the projection of the gradient of the potential on the ground state normal mode surface. To gain insight into the mechanism of the resonance Raman scattering observed for DMU and 5BrDMU, we have calculated the relative resonance Raman intensities of DMU and 5BrDMU in acetonitrile by using both CIS and TD-DFT methods, and the results are listed in Tables S2 and S3 (Supporting Information). The TD-B3LYP method is well known to better predict the electronic correlation. Surprisingly, a huge discrepancy exists between the observed relative resonance Raman intensities and the TD-B3LYP calculated ones for DMU and 5BrDMU in acetonitrile, especially for the ν_7 and ν_9 intensities.

Previous studies have demonstrated that there is a reasonable consistency between the ab initio calculated and the experimental measured relative intensities of n-methylacetamide (NMA)[41] or iodocyclopentane (ICP).[42] To understand the huge discrepancy, we examine the gradient calculations for NMA, ICP, DMU, and 5BrDMU and find that the gradient for NMA and ICP are obtained from a single nondegenerate state having single orbital transition and without significant vibronic coupling between the adjacent electronic states. However, the gradient calculation for DMU in acetonitrile differs in three aspects. First, there exists the overlap between the S_π and the adjacent S_n state due to very close in energy, and both the S_π and S_n states are due to the multiple excitations. Moreover the numbers of the orbital transitions and the corresponding coefficients are very sensitive to the geometry deviations during gradient searching. More importantly the oscillator strengths for the S_π and the adjacent S_n reverse randomly during the calculation. This indicates that the gradient calculated for DMU is not specific to the interested S_π state but instead be mixed by the nearby S_n state due to the strong S_π−S_n vibronic-coupling. Obviously the deviation from a single nondegenerate state makes the TD-B3LYP calculation failure to reproduce the relative experimental resonance Raman intensity pattern for DMU. Different from DMU, the S_n of 5BrDMU in acetonitrile does not overlap with the adjacent S_π state due to the increased energy gap, and the numbers as well as the corresponding coefficients of the multi orbital transitions for 5BrDMU are much less sensitive the geometry changes, the oscillator strengths of the adjacent state remains unaltered during the calculation. This leads to the improved consistency between the calculated and the experimental for 5BrDMU. As is expected, a single nondegenerate state having single orbital transition and without overlapping with the adjacent states is one of the prerequisites for resulting in the accurate prediction of the relative resonance Raman intensities using quantum mechanical calculations.

3.6. Excited State Structures and Reaction Dynamics of DMU. As we focus on the state-mixing and/or conical intersection in FC region, we set our calculations on the singlet $^1\pi\pi^*$ excited states of DMU in which the structural dynamics initiates. Figure 6 displays the CASSCF and TD-B3LYP/6-31G(d) predicted partial potential energy surfaces of DMU.

dx.doi.org/10.1021/jp403798d | J. Phys. Chem. B 2013, 117, 11660−11669

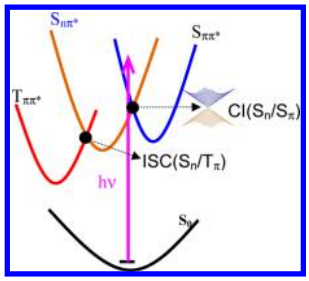

Figure 6. CASSCF and TD-B3LYP/6-31G(d) predicted partial potential energy surfaces of DMU.

The minimum geometric structures of S_n and S_π states are calculated at the TD-B3LYP/6-31G(d) level of theory. The S_n and S_π states are respectively higher in energy than S_0 state by 93 and 107 kcal/mol, but lower in energy than $S_{n,\,FC}$ and $S_{\pi,\,FC}$ by 14.9 and 10.3 kcal/mol. The calculated results indicate that the S_n state is relatively a pure $^1n\pi^*$ state, while the S_π state is noticeably mixed by the S_n state. The important conical intersection point S_n/S_π is predicted at the CASSCF(8,7)/6-31G(d) level of theory, and it is in energy higher than S_0 by 130 kcal/mol. Due to the limited computational resources, we are unable to check the S_n/S_π conical intersection point at any higher theoretical level. Our calculation results indicate that the S_n/S_π conical intersection locates nearby the FC region, and the strong S_n-S_π vibronic-coupling contributes the A-band resonance Raman spectra that displays the significant structural dynamics along the C2═O/C4═O symmetric stretch mode ν_7 and the C2═O/C4═O antisymmetric stretch + C5═C6 stretch mode ν_8. The $S_n/T_1(^3\pi\pi^*)$ intersystem crossing point is predicted in energy higher than S_0 by 85.5 kcal/mol at the CASSCF (8,7)/6-31G(d) level of theory. This indicates that upon excitation, the initially populated S_π state can decay to the lower-lying S_n state and then to the $T_1(^3\pi\pi^*)$ state through the $S_n/T_1(^3\pi\pi^*)$ intersystem crossing point.

It is worth pointing out that the ultrafast radiationless decays of photoexcited uracils were previously investigated by ab initio quantum chemical methods.[44,45] The calculated potential energy profiles indicate that the $S_1\rightarrow S_0$ internal conversion of the pyrimidine bases occurs through a barrierless state switch from the initially excited $^1\pi\pi^*$ state to the out-of-plane deformed excited state of biradical character, which intersects the ground state at a lower energy. That the direct S_0/S_π internal conversion decay to the ground state via strongly out-of-plane distorted geometry (biradical) is the primary ultrafast decay channel for the pyrimidine bases is apparently not mutually exclusive to our present conclusion that the decay dynamics via the S_n/S_π conical intersection in or nearby the Franck−Condon region and the subsequent $S_n/T_1(^3\pi\pi^*)$ intersystem crossing exists for DMU and 5BrDMU, which is actually similar to the previous conclusion that the S_n/S_π crossing mechanism is roughly an order of magnitude slower than the direct S_0/S_π decay for uracil.[44,45]

Further works are required to clarify the role of N-methylation in tuning the energy barrier for the initial state switch, and thus the decay dynamics of uracil. Previous resonance Raman experimental studies in conjunction with time-dependent wave packet theory in simple model[31,32] have been carried out to examine the initial photochemical reaction coordinates of thymine, uracil, 5-halouracil (5-XU, X = F, Cl, and Br) and 1-methyluracil nucleobases in water.[31−35] Kramers−Kronig transform theory has also used to calculate, ab initio, the excitation profiles of resonance Raman active normal coordinates Q_j.[36−38] These studies have provided us preliminary information on the reaction coordinates confined to the S_π state. However, our present study demonstrates that the quantitative modeling of the resonance Raman intensities of various pyrimidine bases need more sophisticated programs like the time-dependent wave packet theory in nonadiabatic realm (multiple excited states) rather than in simple model (one ground state and one excited state) to obtain the normal mode displacements characteristic to the individual S_π state and S_n state. Examination of the variations of the characteristic displacements in conjunction with the subpicosecond to picosecond excited-state lifetimes can undoubtedly open up a new way to deeper insight into the ultrafast decay channels of pyrimidine bases and the competition between the direct S_π/S_0 decay channel and the indirect decay channel via S_n/S_π and $S_n/T_1(^3\pi\pi^*)$.

4. CONCLUSION

The structural dynamics of DMU and 5BrDMU in the $^1\pi\pi^*$ electronic state that has large oscillator strength are studied by using the resonance Raman spectroscopy and the density-functional theory as well as the CASSCF computations. The UV absorption and the vibrational spectra of DMU and 5BrDMU are assigned on the basis of the experimental measurements and density functional theory calculations. Most of the A-band resonance Raman features of DMU can be assigned as 14 Fanck-Condon active modes: ν_7, ν_8, ν_9, ν_{13}, ν_{15}, ν_{17}, ν_{18}, ν_{19}, ν_{21}, ν_{22}, ν_{23}, ν_{24}, ν_{25}, ν_{26}. Similarly, most of the A-band resonance Raman features of 5BrDMU can be assigned as 13 Fanck-Condon active modes: ν_6, ν_7, ν_8, ν_{11}, ν_{13}, ν_{14}, ν_{16}, ν_{18}, ν_{19}, ν_{20}, ν_{25}, ν_{26}, ν_{27}. Solvents do not significantly affect the A-band short-time structural dynamics of DMU or 5BrDMU.

The effect of the methylation at N1, N3 and C5 sites of pyrimidine ring on the structural dynamics of uracils in different solvents were explored on the basis of their resonance Raman intensity patterns. The C5 methylation of uracil changes greatly the initial structural dynamics of uracil in water but not in acetonitrile, and this demonstrates that the C5 methylation is a key structural factor that manipulates the differentiation of the initial structural dynamics and thus the subsequent formation of CPDs between uracil and thymine in water environment. The N3 and/or N1 methylation can effectively alter the short-time structural dynamics and the subsequent decay channels of uracil.

The relative resonance Raman intensities of DMU and 5BrDMU in acetonitrile are computed by using TD-DFT methods. Huge discrepancy exists between the observed relative resonance Raman intensities and the TD-B3LYP calculated ones for DMU and 5BrDMU in acetonitrile, especially for the ν_7 and ν_9 intensities. It demonstrates that the deviation from a single nondegenerate state makes the TD-B3LYP calculation failure to reproduce the relative experimental resonance Raman intensity pattern for DMU. Therefore a single nondegenerate state having single orbital transition and without overlapping with the adjacent states can serve as one of the prerequisites for resulting in an accurate prediction of the relative resonance Raman intensities using quantum mechanical calculations.

The important conical intersection point S_n/S_π is predicted to locate nearby the FC region by using the CASSCF(8,7)/6-31G(d) level of theory computation. This indicates that the initial populated S_π state can decay efficiently and very quickly

dx.doi.org/10.1021/jp403798d | J. Phys. Chem. B 2013, 117, 11660−11669

to the S_n state through S_n/S_π conical intersection. The strong S_1-S_2 vibronic-coupling in FC region contributes the observed significant structural dynamics along the C2═O/C4═O symmetric stretch mode ν_7 and the C2═O/C4═O antisymmetric stretch + C5═C6 stretch mode ν_8. The $S_n/T_1(^3\pi\pi^*)$ intersystem crossing point is predicted at the CASSCF(8,7)/6-31G(d) level of theory. This indicates that the S_n state is a door-way state through which the $T_1(^3\pi\pi^*)$ state can be populated. The partial decay mechanism of DMU upon photoexcitation is revealed as follows:

$$S_0 \xrightarrow{h\nu} S_\pi \xrightarrow{S_\pi/S_n} S_n \xrightarrow{S_n/T_\pi} T_\pi$$

■ ASSOCIATED CONTENT

Supporting Information

Overview of the 299.1, 282.4, 273.9, 266.0, 245.9, 239.5, and 208.8 nm Resonance Raman spectra of DMU in acetonitrile and water (Figure S1). Experimentally observed and B3LYP/6-31+G(d) computed vibrational frequencies of 5BrDMU (Table S1). Comparison of the experimentally observed and the B3LYP-TD and CIS computed relative resonance Raman intensities of DMU and 5BrDMU in acetonitrile (Tables S2 and S3). This information is available free of charge via the Internet at http://pubs.acs.org.

■ AUTHOR INFORMATION

Corresponding Authors

*Telephone: +86-571-86843699; E-mail: zxm@zstu.edu.cn.
*Telephone: +86-010-58805382; E-mail: fangwh@bnu.edu.cn.

Notes

The authors declare no competing financial interest.

■ ACKNOWLEDGMENTS

This work is supported by grants from NNSFC (No. 21033002 and No. 21273202) and the National Basic Research Program of China (2013CB834604).

■ REFERENCES

(1) Crespo-Hernández, C. E.; Cohen, B.; Hare, P. M.; Kohler, B. Ultrafast Excited-State Dynamics in Nucleic Acids. *Chem. Rev.* **2004**, *104*, 1977−2020.

(2) Pecourt, J.-M. L.; Peon, J.; Kohler, B. Ultrafast Internal Conversion of Electronically Excited RNA and DNA Nucleosides in Water. *J. Am. Chem. Soc.* **2000**, *122*, 9348−9349.

(3) Nikogosyan, D. N.; Angelov, D.; Soep, B.; Lindqvist, L. Direct Measurement of Excited Singlet-State Lifetime in the Homologous Sequence Adenine, Adenosine, Adenosine 5′-monophosphate and in Calf Thymus DNA. *Chem. Phys. Lett.* **1996**, *252*, 322−326.

(4) Reuther, A.; Nikogosyan, D. N.; Laubereau, A. Primary Photochemical Processes in Thymine in Concentrated Aqueous Solution Studied by Femtosecond UV Spectroscopy. *J. Phys. Chem.* **1996**, *100*, 5570−5577.

(5) Reuther, A.; Iglev, H.; Laenen, R.; Laubereau, A. Femtosecond Photo-ionization of Nucleic Acid Bases: Electronic Lifetimes and Electron Yields. *Chem. Phys. Lett.* **2000**, *325*, 360−368.

(6) Pecourt, J.-M. L.; Peon, J.; Kohler, B. DNA Excited-State Dynamics: Ultrafast Internal Conversion and Vibrational Cooling in a Series of Nucleosides. *J. Am. Chem. Soc.* **2001**, *123*, 10370−10378.

(7) Gustavsson, T.; Sharonov, A.; Markovitsi, D. Thymine, Thymidine and Thymidine 5′-Monophosphate Studied by Femtosecond Fluorescence Upconversion Spectroscopy. *Chem. Phys. Lett.* **2002**, *351*, 195−200.

(8) Hare, P. M.; Crespo-Hernández, C. E.; Kohler, B. Internal Conversion to the Electronic Ground State Occurs via Two Distinct Pathways for Pyrimidine Bases in Aqueous Solution. *Proc. Natl. Acad. Sci. U.S.A.* **2007**, *104*, 435−440.

(9) Hare, P. M.; Crespo-Hernández, C. E.; Kohler, B. Solvent-Dependent Photophysics of 1-Cyclohexyluracil: Ultrafast Branching in the Initial Bright State Leads Nonradiatively to the Electronic Ground State and a Long-Lived $^1n\pi^*$ State. *J. Phys. Chem. B* **2006**, *110*, 18641−18650.

(10) Kwok, W.-M.; Ma, C.; Phillips, D. L. A Doorway State Leads to Photostability or Triplet Photodamage in Thymine DNA. *J. Am. Chem. Soc.* **2008**, *130*, 5131−5139.

(11) Marguet, S.; Markovitsi, D. Time-Resolved Study of Thymine Dimer Formation. *J. Am. Chem. Soc.* **2005**, *127*, 5780−5781.

(12) Lorentzon, J.; Fuelscher, M. P.; Roos, B. O. Theoretical Study of the Electronic Spectra of Uracil and Thymine. *J. Am. Chem. Soc.* **1995**, *117*, 9265−9273.

(13) Broo, A.; Holmén, A. Calculations and Characterization of the Electronic Spectra of DNA Bases Based on *ab Initio* MP2 Geometries of Different Tautomeric Forms. *J. Phys. Chem. A* **1997**, *101*, 3589−3600.

(14) Gustavsson, T.; Bányász, Á.; Lazzarotto, E.; Markovitsi, D.; Scalmani, G.; Frisch, M. J.; Barone, V.; Improta, R. Singlet Excited-State Behavior of Uracil and Thymine in Aqueous Solution: A Combined Experimental and Computational Study of 11 Uracil Derivatives. *J. Am. Chem. Soc.* **2006**, *128*, 607−619.

(15) Perun, S.; Sobolewski, A. L.; Domcke, W. Conical Intersections in Thymine. *J. Phys. Chem. A* **2006**, *110*, 13238−13244.

(16) Merchán, M.; Serrano-Andrés, L.; Robb, M. A.; Blancafort, L. Triplet-State Formation along the Ultrafast Decay of Excited Singlet Cytosine. *J. Am. Chem. Soc.* **2005**, *127*, 1820−1825.

(17) Blancafort, L.; Robb, M. A. Key Role of a Threefold State Crossing in the Ultrafast Decay of Electronically Excited Cytosine. *J. Phys. Chem. A* **2004**, *108*, 10609−10614.

(18) Improta, R.; Barone, V. Absorption and Fluorescence Spectra of Uracil in the Gas Phase and in Aqueous Solution: A TD-DFT Quantum Mechanical Study. *J. Am. Chem. Soc.* **2004**, *126*, 14320−14321.

(19) Matsika, S. Radiationless Decay of Excited States of Uracil through Conical Intersections. *J. Phys. Chem. A* **2004**, *108*, 7584−7590.

(20) Matsika, S. Three-State Conical Intersections in Nucleic Acid Bases. *J. Phys. Chem. A* **2005**, *109*, 7538−7545.

(21) Marian, C. M.; Schneider, F.; Kleinschmidt, M.; Tatchen, J. Electronic Excitation and Singlet−Triplet Coupling in Uracil Tautomers and Uracil−Water Complexes. *Eur. Phys. J.* **2002**, *D20*, 357−367.

(22) Marian, C. M. A New Pathway for the Rapid Decay of Electronically Excited Adenine. *J. Chem. Phys.* **2005**, *122*, 104314−1−13.

(23) Lim, E. C. Proximity Effect in Molecular Photophysics: Dynamical Consequences of Pseudo-Jahn−Teller Interaction. *J. Phys. Chem.* **1986**, *90*, 6770−6777.

(24) Lai, T.-I.; Lim, E. C. Photophysical Behavior of Aromatic Carbonyl Compounds Related to Proximity Effect: Thioxanthone. *Chem. Phys. Lett.* **1980**, *73*, 244−248.

(25) Broo, A. A Theoretical Investigation of the Physical Reason for the Very Different Luminescence Properties of the Two Isomers Adenine and 2-Aminopurine. *J. Phys. Chem. A* **1998**, *102*, 526−531.

(26) Mennucci, B.; Toniolo, A.; Tomasi, J. Theoretical Study of Guanine from Gas Phase to Aqueous Solution: Role of Tautomerism and Its Implications in Absorption and Emission Spectra. *J. Phys. Chem. A* **2001**, *105*, 7126−7134.

(27) Gustavsson, T.; Sarkar, N.; Lazzarotto, E.; Markovitsi, D.; Barone, V.; Improta, R. Solvent Effect on the Singlet Excited-state Dynamics of 5-Fluorouracil in Acetonitrile as Compared with Water. *J. Phys. Chem. B* **2006**, *110*, 12843−12847.

(28) Gustavsson, T.; Sarkar, N.; Lazzarotto, E.; Markovitsi, D.; Barone, V.; Improta, R. Singlet Excited State Dynamics of Uracil and Thymine Derivatives: A Femtosecond Fluorescence Upconversion Study in Acetonitrile. *Chem. Phys. Lett.* **2006**, *429*, 551−557.

(29) Gustavsson, T.; Bányász, Á.; Sarkar, N.; Markovitsi, D.; Improta, R. Assessing Solvent Effects on the Singlet Excited State Lifetime of Uracil Derivatives: A Femtosecond Fluorescence Upconversion Study in Alcohols and D_2O. *Chem. Phys.* **2008**, *350*, 186−192.
(30) Santoro, F.; Barone, V.; Gustavsson, T.; Improta, R. Solvent Effect on the Singlet Excited-State Lifetimes of Nucleic Acid Bases: A Computational Study of 5-Fluorouracil and Uracil in Acetonitrile and Water. *J. Am. Chem. Soc.* **2006**, *128*, 16312−16322.
(31) Billinghurst, B. E.; Yeung, R.; Loppnow, G. R. Excited-State Structural Dynamics of 5-Fluorouracil. *J. Phys. Chem. A* **2006**, *110*, 6185−6191.
(32) Yarasi, S.; Brost, P.; Loppnow, G. R. Initial Excited-State Structural Dynamics of Thymine Are Coincident with the Expected Photochemical Dynamics. *J. Phys. Chem. A* **2007**, *111*, 5130−5135.
(33) Zhu, X.-M.; Wang, H.-G.; Zheng, X.; Phillips, D. L. Role of Ribose in the Initial Excited State Structural Dynamics of Thymidine in Water Solution: A Resonance Raman and Density Functional Theory Investigation. *J. Phys. Chem. B* **2008**, *112*, 15828−15836.
(34) Yarasi, S.; Ng, S.; Loppnow, G. R. Initial Excited-State Structural Dynamics of Uracil from Resonance Raman Spectroscopy Are Different from Those of Thymine (5-Methyluracil). *J. Phys. Chem. B* **2009**, *113*, 14336−14342.
(35) Weng, K. F.; Wang, H. G.; Zhu, X. M.; Zheng, X. Resonance Raman Spectra of Uracil and 5-Chlorouracil Dynamic Structures during $^1S_0 \rightarrow {}^1S_2$ Transition. *Acta Phys. Chim. Sin.* **2009**, *25*, 1799−1805.
(36) Blazej, D.; Peticolas, W. L. Ultraviolet Resonance Raman Excitation Profiles of Pyrimidine Nucleotides. *J. Chem. Phys.* **1980**, *72*, 3134−3142.
(37) Chinsky, L.; Laigle, A.; Peticolas, W. L.; Turpin, P. Excited State Geometry of Uracil from the Resonant Raman Overtone Spectrum Using a Kramers−Kronig Technique. *J. Chem. Phys.* **1982**, *76*, 1−5.
(38) Peticolas, W. L.; Rush, T. *Ab initio* Calculations of the Ultraviolet Resonance Raman Spectra of Uracil. *J. Comput. Chem.* **1995**, *16*, 1261−1270.
(39) Zheng, X.; Li, Y. L.; Phillips, D. L. Resonance Raman Study of the Short-Time Photodissociation Dynamics of the A-Band Absorption of Cyclopropyl Iodide in Cyclohexane Solution. *J. Phys. Chem. A.* **2004**, *108*, 8032−8039.
(40) Frisch, M. J.; Trucks, G. W.; Schlegel, H. B.; Scuseria, G. E.; Robb, M. A.; Cheeseman, J. R.; Montgomery, J. A., Jr.; Vreven, T.; Kudin, K. N.; Burant, J. C.; et al. *Gaussian 03*, revision B.05; Gaussian, Inc.: Pittsburgh, PA, 2003.
(41) Markham, L. M.; Hudson, B. S. *Ab Initio* Analysis of the Effects of Aqueous Solvation on the Resonance Raman Intensities of *N*-Methylacetamide. *J. Phys. Chem.* **1996**, *100*, 2731−2737.
(42) Zheng, X.; Lee, C. W.; Phillips, D. L. Resonance Raman Study of the *A*-band Short-Time Photodissociation Dynamics of Axial and Equatorial Conformers of Iodocyclopentane. *J. Chem. Phys.* **1999**, *111*, 11034−11043.
(43) Billinghurst, B. E.; Oladepo, S. A.; Loppnow, G. R. Initial Excited-State Structural Dynamics of Thymine Derivatives. *J. Phys. Chem. B* **2012**, *116*, 10496−10503.
(44) Zgierski, M. Z.; Patchkovskii, S.; Fujiwara, T.; Lim, E. C. On the Origin of the Ultrafast Internal Conversion of Electronically Excited Pyrimidine Bases. *J. Phys. Chem. A.* **2005**, *109*, 9384−9387.
(45) Zgierski, M. Z.; Fujiwara, T.; Kofron, W. G.; Lim, E. C. Highly Effective Quenching of the Ultrafast Radiationless Decay of Photo-excited Pyrimidine Bases by Covalent Modification: Photophysics of 5,6-Trimethylenecytosine and 5,6-Trimethyleneuracil. *Phys. Chem. Chem. Phys.* **2007**, *9*, 3206−3209.